SIMULATION AND EXPERIMENTAL ANALYSIS OF CRYSTALLITE SIZE AND MACROSTRAIN OF HEMATITE (Fe₂O₃) NANOPARTICLES USING WILLIAMSON-HALL METHOD

**[*][1]Idris Muhammad Chiromawa, [1]Ibrahim Garba Shitu, [1]Aminu Muhammad,
[2,3]Kamil Kayode Katibi and [1]Sani Garba Durmin Iya**

[1]Department of Physics, Faculty of Natural and Applied Sciences, Sule Lamido Universiti Kafin Hausa, Jigawa State, 048, Nigeria.
[2]Department of Physics, Faculty of Science, Universiti Putra Malaysia, UPM Serdang, Selangor 43400, Malaysia.
[3]Department of Agricultural and Biological Engineering, Faculty of Engineering and Technology, Kwara State University, Malete, 23431, Nigeria.

*Corresponding authors' email: idrismc@slu.edu.ng

ABSTRACT

Determining the crystallite size of nanoparticles represents a significant challenge due to the limitations associated with using a single estimation method. This study addresses this challenge by examining the structural properties of synthesized hematite (Fe₂O₃) nanoparticles through a combination of experimental and simulated X-ray diffraction analyzes (XRD). Using VESTA software, a simulated XRD pattern was created based on precise crystal structure details from a CIF file, accurately confirming the high purity and crystallinity of the synthesized hematite nanoparticles. Various Williamson-Hall models, including the Uniform Deformation Model (UDM), the Uniform Stress Deformation Model (USDM), and the Uniform Stress Energy Density Model (USEDM), were used to estimate crystallite size and microstrain. Comparing the results of both experimental and simulated data revealed slight variations attributed to differences in measurement techniques, sample preparation, and material properties. Furthermore, energy dispersive X-ray (EDX) analysis confirmed the elemental composition of the synthesized nanoparticles, while transmission electron microscopy (TEM) and field emission scanning electron microscopy (FESEM) provided further validation of the particle size. This study provides a comprehensive investigation of the structural properties of hematite nanoparticles (Fe₂O₃) and highlights the importance of integrating multiple analytical techniques and simulation methods to improve the precision and reliability of crystallite size estimation.

Keywords: Hematite (Fe₂O₃), Nanoparticle, Crystallite size, Microstrain, Simulation, Williamson-Hall Model

INTRODUCTION

In recent years, the low combustion synthesis technique has emerged as a highly effective method for producing a wide range of simple and mixed metal oxide nanomaterials. Among these, the auto combustion method has proven particularly successful in fabricating diverse structures such as perovskites, ferrites, aluminates, silicates, and zirconia. This method relies on a self-sustaining ignition reaction between an oxidizer and a fuel in an aqueous solution, which is activated at relatively low temperatures (Prasad et al., 2018). The oxidizer-to-fuel molar ratio (O/F) is meticulously calculated based on the total oxidizing and reducing valencies of the metal nitrate and fuel components (e.g., Fe = +3, O = −2, N = 0, H = +1, and C = +4). Achieving the ideal (O:F) ratio is essential for ensuring efficient combustion synthesis, leading to the production of the desired metal oxides with high purity. The auto combustion synthesis method is widely valued for its simplicity, rapid synthesis, short processing time, and low energy requirements (Fang et al., 2020). Additionally, it is considered environmentally friendly due to its benign nature. This technique enables the fabrication of highly pure, uniformly structured, and crystalline nanoparticles, with versatile shapes and sizes that are suitable for various applications in nanotechnology. The method's ability to produce materials with precise control over their properties makes it an attractive option for researchers and industries alike, catering to the growing demand for advanced nanomaterials. (Pawar et al., 2015)

Hematite nanoparticles, specifically Fe₂O₃, have gained significant attention as versatile nanomaterials with broad applicability in various scientific and technical fields. These nanoparticles possess several advantageous characteristics, including thermodynamic stability, cost-effectiveness, non-toxicity, and remarkable magnetic, electronic, photonic, and optical properties (Liu et al., 2015). Due to these attributes, Fe₂O₃ nanoparticles have been effectively utilized in a wide range of applications, such as gas sensors, biomedical devices, photoanodes, paints, catalysis, building materials, and Li-ion batteries. Their unique combination of properties makes them particularly valuable for advancing technologies in these diverse areas (Devesa et al., 2021a) .

Among the methodologies available for determining crystallite size, Scherrer's method is a well-established technique that uses X-ray diffraction (XRD) patterns to estimate the average size of crystallites based on the width of diffraction peaks. However, it is important to note that Scherrer's formula only provides a lower limit estimation of crystallite size, as it does not account for peak broadening contributions from factors such as inhomogeneous strain and instrumental effects. In practice, both crystallite size and lattice strain contribute to the broadening of X-ray diffraction peaks in nanoparticles. This peak broadening, largely due to lattice strain, is influenced by the significant volume of grain boundaries present in nanoparticles, which can affect the accurate determination of crystallite size. Therefore, it is essential to perform strain calculations to obtain precise measurements of crystallite size and to understand the impact of strain on the properties of nanomaterials (Mote et al., 2012).

In contrast to Scherrer's method, X-ray diffraction peak profile analysis (XPPA) considers peak broadening resulting from inhomogeneous strain and instrumental effects. This comprehensive analytical approach is widely used for determining various parameters in nanocrystalline materials,

including grain size, lattice distortion, twinning, stacking fault probabilities, as well as long-range and root mean square stresses. Williamson-Hall models, in particular, have been employed to estimate both crystallite size and lattice strain by analysing the broadening of X-ray peaks, offering a more nuanced and accurate assessment of the structural properties of nanoparticles (Chandekar & Kant, 2018).

The primary objective of this research is to accurately determine the crystallite size of nanocrystalline hematite (Fe_2O_3) nanoparticles through a comprehensive analysis of powder X-ray diffraction (XRD) data. In addition to examining experimental XRD data, the study will employ VESTA software to simulate the XRD patterns, enabling a comparison between simulated and experimental results to validate the accuracy of the calculated crystallite size. Furthermore, the research will extend its analysis by comparing the crystallite size determined from XRD data with particle size distributions obtained from Transmission Electron Microscopy (TEM) and Field Emission Scanning Electron Microscopy (FESEM) analyses. This multifaceted approach ensures robust validation of the crystallite size and provides a deeper understanding of the structural properties of hematite nanoparticles. By integrating these diverse methodologies, the study aims to offer valuable insights into the structural characterization of nanomaterials, thereby advancing the knowledge base in the field of nanomaterial synthesis and characterization.

MATERIALS AND METHODS
Materials
The materials used in the present research include iron (III) nitrate hydrate Fe $(NO_3)_3 \cdot 9H_2O$ (MW: 404.00; CAS: 7782-61-8), anhydrous citric acid ($C_6H_8O_7.H_2O$) (Mw: 192.12; CAS: 77-92-9), as starting materials and were of analytical grade. Distilled water was used to prepare aqueous solutions during the whole experiment.

Synthesis of Hematite (Fe_2O_3) using Auto-Combustion Technique
Hematite (Fe_2O_3) nanoparticles were synthesized using a straightforward nitrate-citrate sol-gel auto-combustion method. Iron (III) nitrate hydrate ($Fe(NO_3)_3 \cdot 9H_2O$) and citric acid ($C_6H_8O_7 \cdot H_2O$) served as the starting materials, with distilled water and ethanol acting as the solvents. Initially, the precise amounts of the starting precursors were carefully measured using a precision balance. Iron (III) nitrate was then dissolved in 50 ml of distilled water, and the solution was magnetically stirred for 20 minutes to ensure thorough mixing. To enhance the reduction process, an appropriate amount of ethanol was added to the solution. Following this, a small amount of ammonia solution (NH_4OH) was gradually added dropwise, with continuous stirring at room temperature, to adjust the pH of the solution to 7. After the pH adjustment, citric acid was introduced into the solution in a stoichiometric ratio of 1:2 relative to the metal salt. The solution was then heated to 80°C for 2 hours while being continuously stirred with a magnetic stirrer, leading to the formation of a homogeneous mixture. This mixture was further heated to 110°C, converting the sol into a red gel. The temperature was subsequently raised to 250°C to initiate the combustion process. The resulting powdery residue was subjected to a sintering process at 550°C for 5 hours to remove any remaining organic components and to produce dried hematite (Fe_2O_3) nanoparticles.

Simulation of Hematite (Fe_2O_3) using Vesta Software
In this study, the simulation of X-ray diffraction (XRD) patterns for hematite nanoparticles was thoroughly conducted using VESTA software. The procedure began with the download and installation of VESTA, followed by obtaining a CIF (Crystallographic Information File) containing precise crystal structure details for hematite nanoparticles. This CIF file was then imported into VESTA, where simulation parameters were configured, including the specification of the X-ray wavelength and adjustments of other relevant settings to align with the research objectives. The XRD simulation process was subsequently initiated, resulting in the generation of a simulated XRD pattern based on the specified parameters and the crystal structure of the hematite nanoparticles. The analysis of the simulated pattern allowed for the identification of peaks corresponding to the crystallographic planes of hematite. A comparison between the simulated pattern and experimental data was carried out to validate the results, with any necessary adjustments to parameters made to enhance accuracy. Once the simulation was complete, the XRD pattern was saved, and the data were exported for further analysis and documentation. This process provided a comprehensive overview of the simulated structural properties of hematite's crystallographic structure, contributing valuable insights into the material's characteristics.

Characterization
The X-ray diffraction (XRD) patterns were acquired using an X-ray diffractometer (X'pert Pro, Panalytical) equipped with CuKα radiation (λ = 0.154187 nm) over a 2θ angle range of 20° to 80°. The collected XRD patterns were analyzed using X'pert High Score Plus software (Version 3.0e, 3.0.5). The surface properties of the prepared samples were analyzed using the ScanAsyst peak force tapping mode on a Bruker Dimension Edge Atomic Force Microscopy (AFM). The morphology of the samples was further examined using field emission scanning electron microscopy (FESEM) (FEI Nova SEM230) at a working distance of 5.2 mm and an accelerating voltage of 10.0 kV. The elemental composition of the samples was characterized using an energy dispersive X-ray (EDX) spectrometer (7353, Oxford Instruments).

RESULTS AND DISCUSSION
X-ray Diffraction (XRD)
Figure 1 presents the X-ray diffraction (XRD) profile of the synthesized hematite nanoparticles, revealing distinct peaks at specific angles: 24.12°, 33.14°, 35.60°, 40.85°, 49.45°, 54.0°, 57.5°, 62.44°, 64.00°, 72.86°, and 75.35°. These peaks correspond to the crystal planes (111), (220), (311), (222), (400), (422), (511), (440), (214), (300), (1010), and (220), respectively. Notably, these peaks closely match the stick pattern of hexagonal hematite nanoparticles listed in the International Crystallographic Diffraction Data (ICDD) under reference number 00-024-0072. The absence of impurity peaks in the diffractogram indicates the high purity of the synthesized particles. Moreover, the sharpness of the diffraction peaks suggests that the particles are highly crystalline. Utilizing this diffraction profile, we can proceed to calculate essential parameters such as crystallite size, intrinsic strain, and stress of the nanoparticles. These calculations will be conducted using various models, as described in the following sections, to ensure a comprehensive analysis of the structural properties of the synthesized hematite nanoparticles.
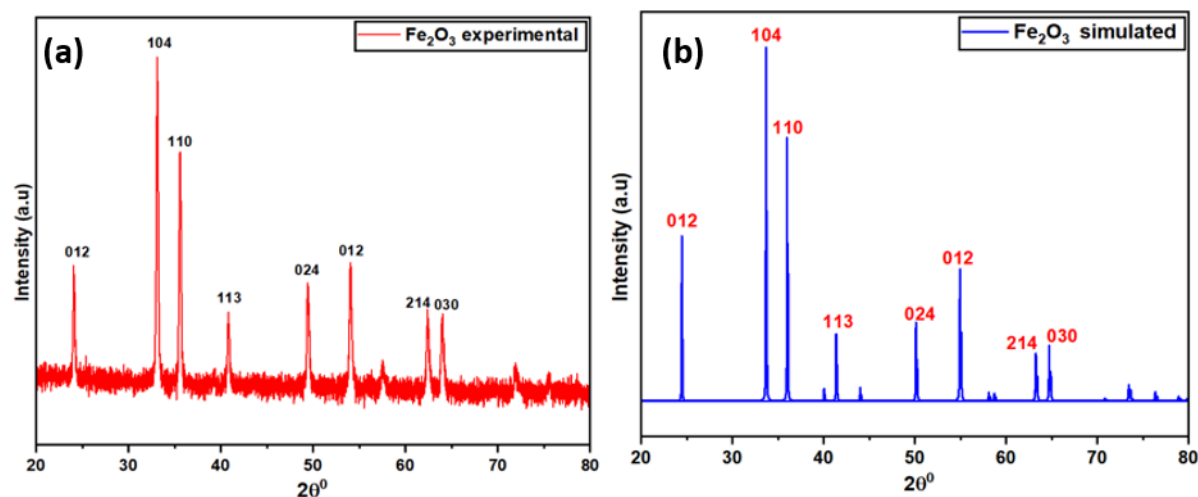
Figure 1: (a) Experimental data (b) Simulated data

Scherer's Method

The Scherrer method, also known as the Scherrer equation or Scherrer formula, is widely used for estimating crystallite size in a material based on the broadening of X-ray diffraction peaks. This method provides valuable insight into the average size of the crystalline domains present in a sample (Shitu et al., 2021). The Scherrer equation is derived from the basic principles of X-ray diffraction and exploits the peak broadening that results from the finite size of crystalline domains. According to this Equation, the crystallite size (D) is related to the peak broadening (β), the X-ray wavelength (λ), the Bragg angle (θ), and the dimensionless form factor (K)(Yao et al., 2017) :

$$D = \frac{k\lambda}{\beta_{hkl}\cos\theta} \qquad (1)$$

X-ray wavelength, k (often considered to be 0.9), β_{hkl} is the FWHM (full width at half maximum) of the diffraction peaks, and θ is the Bragg's angle of reflection.

Scherrer's method involves X-ray diffraction (XRD) measurements on Fe_2O_3 nanoparticles. The resulting XRD patterns indicate the positions and intensities of the diffraction peaks, which correlate with the crystal planes in the material. Since the crystalline domains have finite sizes, the peaks show broadening due to the size effect (Kumar et al., 2020). Figure 2 illustrates the use of the Scherer method to estimate the crystallite size and microstrain Fe_2O_3 nanoparticles of both experimental and simulated data. The calculated crystallite sizes and microstrain were determined to be 43.33 and 46.06, and 2.6×10^{-3} and 1.75×10^{-3}, respectively, corresponding to experimental and simulated data for Fe_2O_3 nanoparticles. It is noted that the experimental crystallite size and microstrain of Fe_2O_3 nanoparticles are marginally smaller than the simulated results, possibly due to factors such as differences in sample preparation methods, surface effects, and the presence of defects not accurately accounted for in simulations (Maniammal et al., 2017). Additionally, variations in experimental conditions, including synthesis techniques and environmental factors, may introduce complexities impacting the measured parameters. Moreover, limitations in experimental equipment or data analysis techniques could also contribute to disparities between experimental and simulated outcomes (Devesa et al., 2021b).
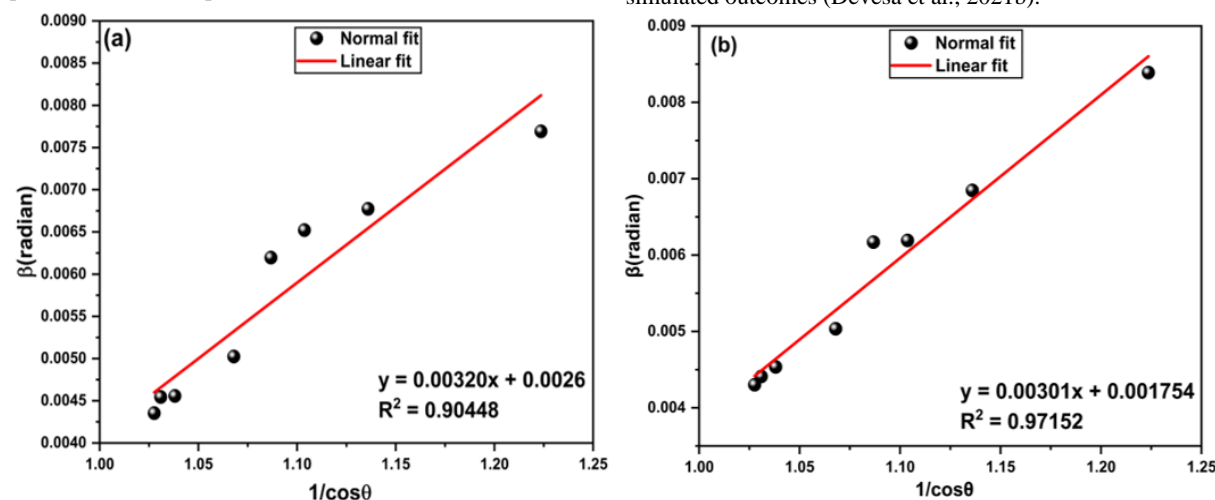
Figure 2: Fe_2O_3 nanoparticles crystallite size and microstrain plots using Scherer's method (a) experimental data (b) simulated data

Williamson-Hall Method (WHM)

The Scherrer equation, which is used to describe the influence of crystallite size on X-ray diffraction (XRD) peak broadening, is limited in its ability to assess intrinsic strain caused by factors such as point defects, grain boundaries, triple junctions, and stacking faults within nanocrystals (Thandavan et al., 2015). Unlike the Scherrer equation, the Williamson-Hall method considers the effect of strain-induced XRD peak broadening and is capable of evaluating both crystal size and intrinsic strain. Whereas the Scherrer

equation relies on 1/cosθ dependence, the Williamson-Hall method deviates from this by incorporating tanθ term to account for strain effects (Al-Tabbakh et al., 2019). This fundamental difference allows the Williamson-Hall method to separate the contributions of microstrain and crystallite size to peak broadening. The accuracy of this method, however, depends on several factors, including the quality of the XRD pattern, the shape factor, and assumptions made about the crystal structure (Monshi et al., 2012). The overall broadening of XRD peaks, resulting from the combined effects of crystallite size and intrinsic strain in nanocrystals, can be represented by the following expression (Bodke et al., 2018):

$$\beta_{hkl} = (\beta_{size} - \beta_{strain}) \qquad (2)$$

Here, β_{size} β_{Strain} the XRD full width at half maximum (FWHM) is due to the microstrain and size of the nanoparticle. The modified Williamson-Hall method (W-H) encompasses three models: Uniform Deformation Model (UDM), Uniform Stress Deformation Model (USDM), and Uniform Stress Energy Density Model (UDEDM). This research applied all these models to compute the mean crystallite size and microstrain of Fe_2O_3 nanoparticles synthesized using the microwave-assisted hydrothermal technique.

Uniform Deformation Model (UDM)

The Williamson-Hall technique, commonly used to determine crystallite dimensions and lattice distortions in materials from X-ray diffraction (XRD) data, can be extended through the inclusion of the Uniform Deformation Model (UDM). This extension allows for a more comprehensive analysis by considering both size-related variations and strain-induced effects on peak broadening (Kong et al., 2019). The UDM posits that lattice strain and crystallite size contribute independently to the broadening observed in XRD peaks. This model accounts for the effects of microstructural imperfections and lattice distortions within the crystalline domains. Peak broadening due to size variation arises from the finite dimensions of the crystalline regions, while stress-induced broadening results from distortions or microstrain within the material (Zhou et al., 2018). The broadening of X-ray diffraction peaks due to inherent strain, which increases the line widths, can be mathematically expressed as follows (Nath et al., 2020):

$$\beta_{strain} = 4\varepsilon\sin\theta \qquad (3)$$

The overall XRD peak broadening resulting from the combined influences of size and strain effects across all diffraction planes (hkl) could be expressed mathematically as:

$$\beta_{hkl} = (\beta_{size} - \beta_{strain}) \qquad (4)$$

Where β_{hkl} is the full width at half maximum (FWHM), which characterizes the extension of the diffraction planes (hkl) within the X-ray diffraction spectra (XRD). This parameter applies to either all discernible peaks or particular chosen ones. A while β_{size} could be expressed as:

$$\beta_{size} = \frac{k\lambda}{D} \cdot \frac{1}{\cos\theta}, \qquad (5)$$

and

$$\beta_{strain} = 4\varepsilon\sin\theta. \qquad (6)$$

The expression for UDM can be expressed as follows:

$$\beta_{hkl} = \frac{k\lambda}{D} \cdot \frac{1}{\cos\theta} + 4\varepsilon\sin\theta \qquad (7)$$

Rearranging Equation (00) yields:

$$\beta_{hkl}\cos\theta = \frac{k\lambda}{D} + 4\varepsilon\sin\theta \qquad (9)$$

Equation (9) represents a linear equation based on the Uniform Deformation Model (UDM). Figure 3 displays the plots derived from Equation (9), corresponding to the main diffraction peaks of Fe_2O_3 nanoparticles. The intercept and slope of the linearly fitted plot provide critical information about the inherent strain and mean crystallite dimensions of Fe_2O_3 nanoparticles synthesized under different irradiation durations. The occurrence of lattice strain is primarily attributed to the expansion or contraction of crystal lattices within nanocrystals, a phenomenon largely influenced by the size confinement effect. This effect leads to the expansion or contraction of the crystal lattices, and the restriction in size also introduces imperfections within the lattice structure, further contributing to the lattice strain (Ilyas et al., 2019).

Figure 3 illustrates the uniform deformation model plots for Fe_2O_3 nanoparticles. By applying the uniform deformation model, the mean crystallite sizes and microstrain values of Fe_2O_3 nanoparticles for both experimental and simulated data were determined to be 49.70 nm and 57.75 nm, with corresponding microstrain values of 1.61×10^{-3} and 1.55×10^{-3}, respectively. It is noteworthy that the crystallite size and microstrain values obtained using the UDM model are slightly larger than those obtained using Scherrer's method. This difference highlights the impact of considering lattice strain and microstructural imperfections, which are accounted for in the UDM but not in the simpler Scherrer's method (Garg et al., 2018).
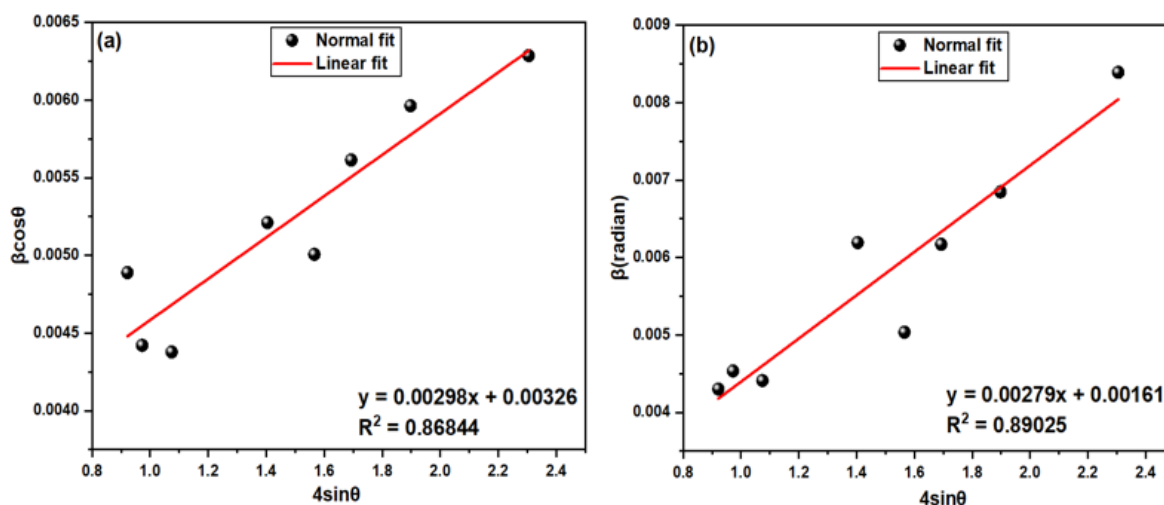
Figure 3: Fe_2O_3 nanoparticles crystallite size and microstrain plots using uniform deformation model (UDM) (a) experimental data (b) simulated data

Uniform Stress Deformation Model (USDM)

To address the presence of anisotropic stress, the Williamson-Hall equation (W-H) has been revised, as the assumption of uniformity and isotropy does not hold universally. This modified approach is known as the Uniform Stress Deformation Model (USDM). Within the USDM framework, strain is considered to be isotropic, while also accounting for minor microstrain. In this model, Hooke's Law establishes a relationship between stress and strain within the crystal lattice, expressed as σ = Eε. Where σ represents stress, ε denotes anisotropic microstrain, and E is Young's modulus(Irfan et al., 2018) . This equation indicates that the stress applied to the crystal is directly proportional to the strain experienced, with EEE serving as the constant of proportionality. However, as the stress increases, the linear correlation may begin to deviate. The adapted form of the Williamson-Hall equation accommodates the impact of stress on all lattice planes (hkl) and can be expressed as follows (Akl & Hassanien, 2014):

$$\beta_{hkl}\cos\theta = \frac{k\lambda}{D} + 4\sigma\frac{\sin\theta}{E_{hkl}} \qquad (9)$$

Equation (9) is recognized as the uniform stress deformation model (USDM). By plotting a graph with $(\beta_{hkl}\cos\theta)$ the y-axis and $4\frac{\sin\theta}{E_{hkl}}$ the x-axis, the uniform stress and the crystallite size (D) can be extracted from the slope and intercept of the plotted graph, as revealed in Figure (8). Moreover, the intrinsic strain can be calculated by considering the strain value and the elastic modulus of Fe_2O_3 nanoparticles across various crystallographic orientations. Within hexagonal structures, Young's modulus can be determined using the formula given (Nath et al., 2020):

$$E_{hkl} = \frac{\left[h^2 + \frac{(h+2k)^2}{3} + \left(\frac{al}{c}\right)^2\right]^2}{S_{11}\left(h^2 + \frac{(h+2k)^2}{3}\right)^2 + S_{33}\left(\frac{al}{c}\right)^4 + (2S_{13}+S_{44})\left(h^2 + \frac{(h+2k)^2}{3}\right)\left(\frac{al}{c}\right)^2} \qquad (10)$$

The formula (Equation (10)) integrates hkl indices representing X-ray diffraction planes, and 'a' and 'c' symbolize the lattice parameters in Fe_2O_3 nanoparticle's hexagonal structure (these values are obtainable from the phase file using X-pert High Score software). Elastic compliances (S_{11}, S_{13}, S_{33}, and S_{44}) of Fe_2O_3 nanoparticles are derived from elastic stiffness constants (C_{11}, C_{13}, C_{33}, and C_{44}). These compliances are represented as follows (Mote et al., 2012):

$$S_{11} = \frac{1}{2}\left[\frac{C_{33}}{C_{33}(C_{11}+C_{12}) - 2(C_{13})^2} + \frac{1}{(C_{11}-C_{12})}\right] \qquad (11)$$

$$S_{13} = \left[\frac{-C_{13}}{C_{33}(C_{11}+C_{12}) - 2(C_{13})^2}\right] \qquad (12)$$

$$S_{33} = \left[\frac{C_{11}+C_{12}}{C_{33}(C_{11}+C_{12}) - 2(C_{13})^2}\right] \qquad (13)$$

$$S_{44} = \frac{1}{C_{44}} \qquad (14)$$

For the hexagonal structure, the modulus of elasticity (Y) is defined by Equation (24), where the elastic constants for zinc oxide are where $S_{11} = 2.234 \times 10^{-12}$ m^2 N^{-1}, $S_{33} = 1.425 \times 10^{-12}$ m^{2}N^{-1}, $S_{13} = 2.329 \times 10^{-12}$ m^{2}N^{-1}, $S_{44} = 0.782 \times 10^{-12}$ m^{2}N^{-1}. The modulus of elasticity (Y) of Fe_2O_3 nanoparticles was calculated to be 173 GPa, which is in close agreement with the modulus of elasticity of Fe_2O_3, measured at 176 GPa.

Using Equation (9), a plot of $(\beta_{hkl}\cos\theta)$ against $4\frac{\sin\theta}{E_{hkl}}$ is shown in Figure 8. From the gradient and intercept of the linear plot, the stress and mean crystallite size of Fe_2O_3 nanoparticles synthesized at different irradiation times were determined. The average particle size was estimated to be 46.02 nm. This result is consistent with the average crystallite size obtained using Scherrer's method from both experimental and simulated XRD data, confirming the reliability of the measurements.

Figure 4: Fe_2O_3 nanoparticles crystallite size and microstrain plots using uniform stress deformation model (USDM) (a) experimental data (b) simulated data

Uniform Stress Energy Density Deformation Model (USEDM)

The Uniform Stress Energy Density Deformation Model (USEDM) is an advanced adaptation of the Williamson-Hall (W-H) method, employed for determining nanoparticle crystallite size from X-ray diffraction (XRD) data. The USEDM model assumes an even distribution of strain within the crystal lattice and takes into account both crystallite size and the inherent stress that contributes to the broadening of XRD peaks (Augustin, 2016). Additionally, this model incorporates the concept of strain energy density, which

provides a measure of the energy required to induce deformation within the crystal structure. The USEDM model has proven to be effective not only in approximating the dimensions of crystallites in nanoparticles through XRD analysis but also in evaluating energy density, stress, and strain parameters within these materials. This approach offers a novel and precise method for calculating stress and strain values, making it highly valuable in the context of materials engineering and development. (Science-poland, 2020) A unique aspect of the USEDM is its integration of the crystal's deformation energy density, a key parameter that relates to the

modulus of elasticity (E), which is critical in engineering applications. Unlike the Uniform Deformation Model (UDM) and the Uniform Stress Deformation Model (USDM), the USEDM model uniquely considers the uniform distribution of stress anisotropy across all diffraction planes, which stems from the intrinsic energy density of the crystal (Sivakami et al., 2016).

According to Hooke's Law, the relationship between energy density (u) and strain (ε) can be expressed as:

$$u = \varepsilon^2 \frac{E_{hkl}}{2} \qquad (15)$$

Furthermore, it is established that stress maintains a linear relationship with strain. Consequently, strain as a function of energy density can be represented in the following:

$$\varepsilon = \sigma \sqrt{\frac{2u}{E_{hkl}}} \qquad (16)$$

Where E_{hkl} is Young's modulus (modulus of elasticity) applicable to all crystallographic directions. Now, upon substituting Equation (14) into Equation (9) provided earlier and rearranging, we arrive at:

$$\beta_{hkl}\cos\theta = \frac{k\lambda}{D} + 4\sigma\sin\theta \sqrt{\frac{2u}{E_{hkl}}} \qquad (17)$$

Equation (17) is in the form of a linear equation and is referred to as the Uniform Strain Energy Density (UDEDM) model. Hence, as illustrated in Figure 5, a linear graph is generated when plotting a graph $(\beta_{hkl}\cos\theta)$ on the y-axis and $\left(4\sin\theta \sqrt{\frac{2u}{E_{hkl}}}\right)$ the x-axis. By analyzing the slope and intercept of the linear fit in this graph, the energy density (u) and average crystallite size (D) of Fe_2O_3 nanoparticles were determined. The intersections of the straight lines provided estimated mean crystallite sizes of 48.65 nm and 63.02 nm for the experimental and simulated Fe_2O_3 nanoparticles, respectively. The slopes of these lines correspond to energy density values of 4.03 KJ/m³ and 1.36 KJ/m³, respectively. It is also noteworthy that the crystallite sizes obtained using the USEDM are slightly larger than those obtained using Scherrer's method. This difference highlights the impact of considering energy density and strain in the calculation, which can lead to a more comprehensive understanding of the material's structural properties (Abed et al., 2019).
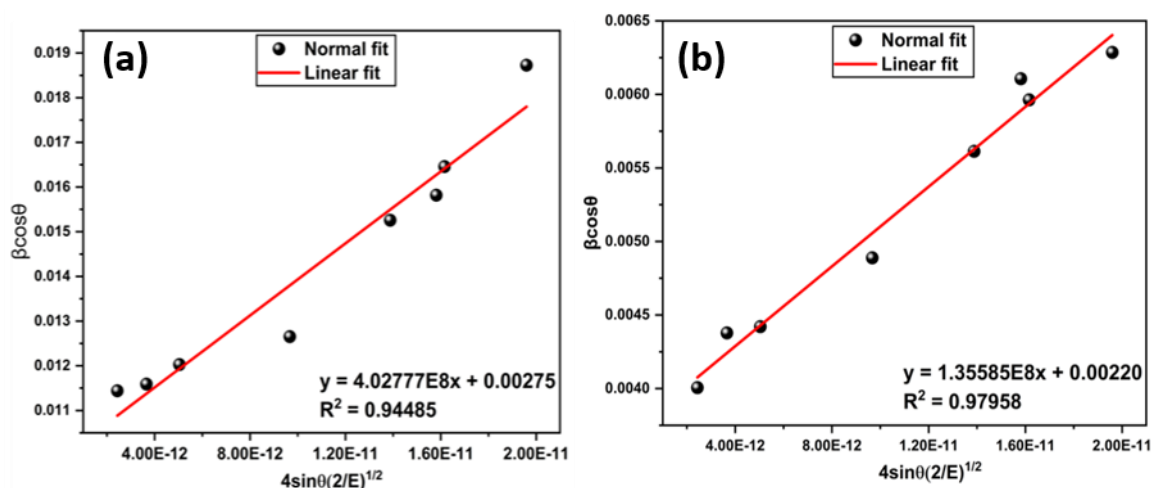
Figure 5: Fe_2O_3 nanoparticles crystallite size and microstrain plots using uniform stress energy deformation model (USEDM) (a) experimental data (b) simulated data

Field Emission Scanning Electron Microscopy (FESEM)

Figure 6(a) presents a field emission scanning electron microscopy (FESEM) image that reveals the morphology of the synthesized nanoparticles, characterized by a densely packed arrangement of spherical particles. The Field Emission Scanning Electron Microscopy (FESEM) image highlights the uniformity of the nanoparticles, showing a consistent size and shape, which indicates a well-controlled synthesis process. Complementing this morphological analysis, Figure 6(b) displays a histogram that represents the particle size distribution derived from the FESEM data. The average particle size is determined to be 46.65 nm, which closely aligns with the crystallite size obtained through both the Williamson-Hall analysis and the Scherrer method. The Williamson-Hall models, which account for both size and strain effects on X-ray diffraction (XRD) peak broadening,

provide a crystallite size estimate that closely matches the particle size observed in FESEM. Similarly, the Scherrer method, which directly relates XRD peak broadening to crystallite size, corroborates this finding. The consistency in particle size across these different characterization methods suggests that the synthesis process was highly effective in controlling the growth of the nanoparticles, resulting in a uniform and well-defined product (Prabhu & Rao, 2014). Such uniformity is essential for applications that require precise control over particle size and crystallinity. The close agreement between the average particle size and the crystallite size across multiple analytical techniques underscores the reliability and effectiveness of the synthesis method employed, highlighting its potential for producing high-quality nanomaterials suitable for advanced technological applications (Abd El-Sadek et al., 2019).
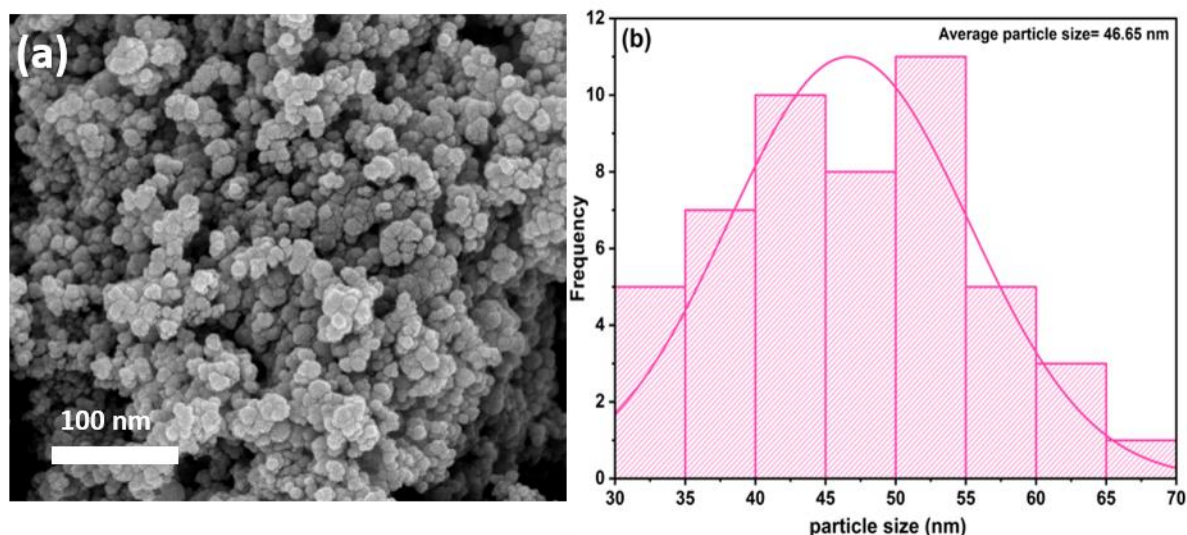
Figure 6: (a) FESEM image (b) size distribution histogram

Transmission Electron Microscopy (TEM)
Figure 7(a) displays a Transmission Electron Microscopy (TEM) image of the nanoparticles, revealing irregular shapes and a range of particle sizes. The scale bar in the image confirms that the nanoparticles are within the nanometre scale, with dimensions below 100 nm. Figure 7(b) complements this visual analysis by presenting a histogram of the particle size distribution obtained from the TEM analysis. The distribution indicates a range of particle sizes, with the average size estimated to be 48.23 nm. This average particle size is consistent with the crystallite size calculated using various Williamson-Hall models, as well as the size estimated using the Scherrer method. The agreement between the particle size determined by TEM and the crystallite size obtained from X-ray diffraction (XRD) methods underscores the reliability and consistency of the synthesis and characterization processes used in this study. The Williamson-Hall analysis, which accounts for both strain and size effects on XRD peak broadening, typically provides an estimate of crystallite size that aligns well with the direct measurements from TEM. Similarly, the Scherrer method, which correlates the broadening of diffraction peaks to crystallite size, corroborates the average size of 48.23 nm observed in the TEM analysis. This consistency across different analytical techniques suggests that the nanoparticles possess a uniform and well-defined size, highlighting the effectiveness of the synthesis method in producing high-quality nanoparticles suitable for various applications (Rajesh Kumar & Hymavathi, 2017).
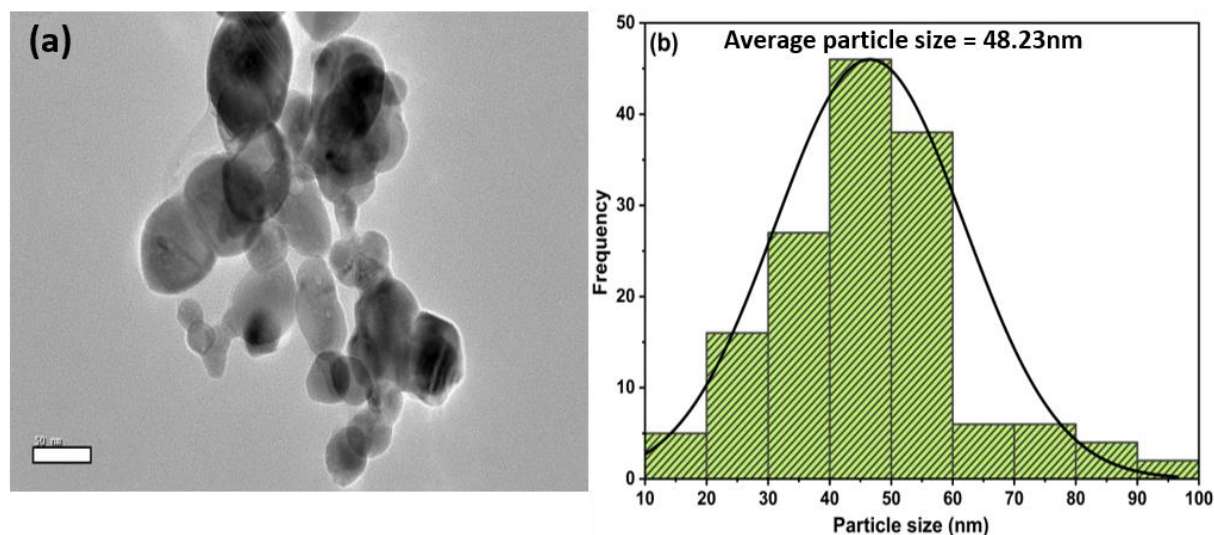
Figure 7: (a) Transmission Electron Microscopy (TEM) image (b) Histogram of the particle size distribution

CONCLUSION
This research investigates the structural properties of synthesized hematite nanoparticles (Fe_2O_3) using experimental and simulated X-ray diffraction (XRD) techniques. The study demonstrated the high purity and crystallinity of the nanoparticles, supported by the close agreement between experimental and simulated XRD patterns. Crystallite size and microstrain were estimated using the Scherrer method, the size strain plot method, and the Halder-Wagner method. Some discrepancies were observed between the experimental and simulated data, which are likely due to inherent differences in measurement techniques and material properties. Further validation of the composition of the nanoparticles was performed by energy dispersive X-ray analysis (EDX), while transmission electron microscopy (TEM) confirmed the particle size estimates. This study

provides comprehensive insights into the structural properties of hematite nanoparticles and emphasizes the importance of using multiple analytical techniques and simulation methods to accurately estimate crystallite size and microstrain. By integrating experimental data with simulation results, the research provides a comprehensive understanding of the composition and structural properties of Fe_2O_3 nanoparticles. The results contribute significantly to the field of nanomaterials research and lay the foundation for future studies and possible applications in various technology areas.

REFERENCES

Abd El-Sadek, M. S., Wasly, H. S., & Batoo, K. M. (2019). X-ray peak profile analysis and optical properties of CdS nanoparticles synthesized via the hydrothermal method. Applied Physics A: Materials Science and Processing, 125(4). https://doi.org/10.1007/s00339-019-2576-y

Abed, A. H., Khodair, Z. T., Al-saadi, T. M., & Al-dhahir, T. A. (2019). Study the evaluation of Williamson – Hall (W- H) strain distribution in silver nanoparticles prepared by sol-gel method Study the Evaluation of Williamson – Hall (W-H) Strain Distribution in Silver Nanoparticles Prepared by Sol-Gel Method. 020019(July).

Akl, A. A., & Hassanien, A. S. (2014). Microstructure characterization of Al-Mg alloys by X-ray diffraction line profile analysis Alloy 5251 Al Si Fe Cu Mn Mg Cr Zn Al Reminder. 2(11), 1–9.

Al-Tabbakh, A. A., Karatepe, N., Al-Zubaidi, A. B., Benchaabane, A., & Mahmood, N. B. (2019). Crystallite size and lattice strain of lithiated spinel material for rechargeable battery by X-ray diffraction peak-broadening analysis. International Journal of Energy Research, 43(5), 1903–1911. https://doi.org/10.1002/er.4390

Augustin, M. (2016). Estimation of Lattice Stress and Strain in Zinc and Manganese Ferrite Nanoparticles by Williamson – Hall and Size-Strain Plot Methods. 15(4), 1–7. https://doi.org/10.1142/S0219581X16500356

Bodke, M., Gawai, U., Patil, A., & Dole, B. (2018). Estimation of accurate size, lattice strain using Williamson-Hall models, SSP and TEM of Al doped ZnO nanocrystals. Materiaux et Techniques, 106(6). https://doi.org/10.1051/mattech/2018055

Chandekar, K. V., & Kant, K. M. (2018). Size-strain analysis and elastic properties of CoFe2O4 nanoplatelets by hydrothermal method. Journal of Molecular Structure, 1154, 418–427. https://doi.org/10.1016/j.molstruc.2017.09.104

Devesa, S., Rooney, A. P., Graça, M. P., Cooper, D., & Costa, L. C. (2021a). Materials Science & Engineering B Williamson-hall analysis in estimation of crystallite size and lattice strain in Bi 1 . 34 Fe 0 . 66 Nb 1 . 34 O 6 . 35 prepared by the sol-gel method. Materials Science & Engineering B, 263(September 2020), 114830. https://doi.org/10.1016/j.mseb.2020.114830

Devesa, S., Rooney, A. P., Graça, M. P., Cooper, D., & Costa, L. C. (2021b). Williamson-hall analysis in estimation of crystallite size and lattice strain in Bi1.34Fe0.66Nb1.34O6.35 prepared by the sol-gel method. Materials Science and Engineering B: Solid-State Materials for Advanced Technology, 263. https://doi.org/10.1016/j.mseb.2020.114830

Fang, H., Guo, H., Hu, Y., Ren, Y., Hsu, P. C., & Bai, S. L. (2020). In-situ grown hollow Fe3O4 onto graphene foam nanocomposites with high EMI shielding effectiveness and thermal conductivity. Composites Science and Technology, 188. https://doi.org/10.1016/j.compscitech.2019.107975

Garg, P., Rai, R., & Singh, B. K. (2018). Structural characterization of "as-deposited" cesium iodide films studied by X-ray di ff raction and transmission electron microscopy techniques.

Ilyas, S., Abdullah, B., & Tahir, D. (2019). Nano-Structures & Nano-Objects X-ray diffraction analysis of nanocomposite Fe 3 O 4 / activated carbon by Williamson – Hall and size-strain plot methods. Nano-Structures & Nano-Objects, 20, 100396. https://doi.org/10.1016/j.nanoso.2019.100396

Irfan, H., K, M. R., & Anand, S. (2018). Microstructural evaluation of CoAl 2 O 4 nanoparticles by Williamson – Hall and size – strain plot methods. Journal of Asian Ceramic Societies, 00(00), 1–9. https://doi.org/10.1080/21870764.2018.1439606

Kong, F., Bai, J., Bi, P., Liu, X., Wang, Z., & Xiong, R. (2019). Size effect enhanced thermoelectric properties of nanoscale Cu 2-x Se. Ceramics International, 45(7), 8866–8872. https://doi.org/10.1016/j.ceramint.2019.01.215

Kumar, R., Youssry, S. M., Abdel-Galeil, M. M., & Matsuda, A. (2020). One-pot synthesis of reduced graphene oxide nanosheets anchored ZnO nanoparticles via microwave approach for electrochemical performance as supercapacitor electrode. Journal of Materials Science: Materials in Electronics, 31(18), 15456–15465. https://doi.org/10.1007/s10854-020-04108-w

Liu, P., Huang, Y., & Zhang, X. (2015). Cubic NiFe2O4 particles on graphene-polyaniline and their enhanced microwave absorption properties. Composites Science and Technology, 107, 54–60. https://doi.org/10.1016/j.compscitech.2014.11.021

Maniammal, K., Madhu, G., & Biju, V. (2017). X-ray diffraction line profile analysis of nanostructured nickel oxide: Shape factor and convolution of crystallite size and microstrain contributions. Physica E: Low-Dimensional Systems and Nanostructures, 85, 214–222. https://doi.org/10.1016/j.physe.2016.08.035

Monshi, A., Foroughi, M. R., & Monshi, M. R. (2012). Modified Scherrer Equation to Estimate More Accurately

Nano-Crystallite Size Using XRD. World Journal of Nano Science and Engineering, 02(03), 154–160. https://doi.org/10.4236/wjnse.2012.23020

Mote, V. D., Purushotham, Y., & Dole, B. N. (2012). Williamson-Hall analysis in estimation of lattice strain in nanometer-sized ZnO particles. 2–9.

Nath, D., Singh, F., & Das, R. (2020). X-ray diffraction analysis by Williamson-Hall, Halder-Wagner and size-strain plot methods of CdSe nanoparticles- a comparative study. Materials Chemistry and Physics, 239(April 2019), 122021. https://doi.org/10.1016/j.matchemphys.2019.122021

Pawar, S. P., Marathe, D. A., Pattabhi, K., & Bose, S. (2015). Electromagnetic interference shielding through MWNT grafted Fe3O4 nanoparticles in PC/SAN blends. Journal of Materials Chemistry A, 3(2), 656–669. https://doi.org/10.1039/c4ta04559a

Prabhu, Y. T., & Rao, K. V. (2014). X-Ray Analysis by Williamson-Hall and Size-Strain Plot Methods of ZnO Nanoparticles with Fuel Variation. March, 21–28.

Prasad, J., Singh, A. K., Shah, J., Kotnala, R. K., & Singh, K. (2018). Synthesis of MoS2-reduced graphene oxide/Fe3O4 nanocomposite for enhanced electromagnetic interference shielding effectiveness. Materials Research Express, 5(5). https://doi.org/10.1088/2053-1591/aac0c2

Rajesh Kumar, B., & Hymavathi, B. (2017). X-ray peak profile analysis of solid-state sintered alumina doped zinc oxide ceramics by Williamson–Hall and size-strain plot methods. Journal of Asian Ceramic Societies, 5(2), 94–103. https://doi.org/10.1016/j.jascer.2017.02.001

Science-poland, M. (2020). X-ray diffraction study of the elastic properties of jagged spherical CdS nanocrystals. 38(2), 271–278. https://doi.org/10.2478/msp-2020-0032

Shitu, I. G., Liew, J. Y. C., Talib, Z. A., Baqiah, H., Awang Kechik, M. M., Ahmad Kamarudin, M., Osman, N. H., Low, Y. J., & Lakin, I. I. (2021). Influence of Irradiation Time on the Structural and Optical Characteristics of CuSe Nanoparticles Synthesized via Microwave-Assisted Technique. ACS Omega, 6(16), 10698–10708. https://doi.org/10.1021/acsomega.1c00148

Sivakami, R., Dhanuskodi, S., & Karvembu, R. (2016). Spectrochimica Acta Part A : Molecular and Biomolecular Spectroscopy Estimation of lattice strain in nanocrystalline RuO 2 by Williamson – Hall and size – strain plot methods. 152, 43–50. https://doi.org/10.1016/j.saa.2015.07.008

Thandavan, T. M. K., Gani, S. M. A., Wong, C. S., & Nor, R. M. (2015). Evaluation of Williamson–Hall Strain and Stress Distribution in ZnO Nanowires Prepared Using Aliphatic Alcohol. Journal of Nondestructive Evaluation, 34(2), 1–9. https://doi.org/10.1007/s10921-015-0286-8

Yao, W. lin, Xiong, G., Yang, Y., Huang, H. qing, & Zhou, Y. fen. (2017). Effect of silica fume and colloidal graphite additions on the EMI shielding effectiveness of nickel fiber cement based composites. Construction and Building Materials, 150, 825–832. https://doi.org/10.1016/j.conbuildmat.2017.06.019

Zhou, R., Huang, Y., Zhou, J., Niu, H., Wan, L., Li, Y., Xu, J., & Xu, J. (2018). Copper selenide (Cu3Se2 and Cu2−xSe) thin films: electrochemical deposition and electrocatalytic application in quantum dot-sensitized solar cells. Dalton Transactions, 47(46), 16587–16595. https://doi.org/10.1039/c8dt03791d